Journal of Materials Chemistry A

ROYAL SOCIETY OF CHEMISTRY

PAPER

View Article Online
View Journal | View Issue

Open Access Article. Published on 15 September 2020. Downloaded on 12/9/2025 1:00:59 AM.
This article is licensed under a Creative Commons Attribution-NonCommercial 3.0 Unported Licence.

Check for updates

Cite this: *J. Mater. Chem. A*, 2020, **8**, 19991

Polyiodide solid-state dye-sensitized solar cell produced from a standard liquid I^-/I_3^- electrolyte†

Ellie Tanaka and Neil Robertson *

Received 28th July 2020
Accepted 14th September 2020

DOI: 10.1039/d0ta07377f

rsc.li/materials-a

Solid-state dye-sensitized solar cells were obtained by drying a standard I^-/I_3^- liquid-electrolyte cell in ambient conditions. Slow evaporation of the organic solvent allows the formation of a polyiodide (I_n^-, $n \geq 3$) network that bridges the counter electrode and dye/TiO_2 layer. The unsealed polyiodide solar cell (Ply-I DSSC) with 5T dye reaches a maximum of 5.2% peak power conversion efficiency (peak PCE), similar to the precursor liquid-state solar cell (Liq-I DSSC) of maximum PCE = 5.7%. Once the performance of the Ply-I DSSCs reaches a stabilization (stb.) point (maximum stb. PCE 5.0%), no loss in performance is displayed under dark storage in ambient air without any encapsulation for a period of around 10 months.

Introduction

Photovoltaic cells consisting of a dye-sensitized wide band gap semiconductor have been researched for more than 50 years, dating back to reports in the 1960s.[1,2] High performance dye-sensitized solar cells (DSSC) over 7% power conversion efficiency (PCE) were first reported by O'Regan and Grätzel in 1991.[3] Their device design included a mesoporous TiO_2 layer and an I^-/I_3^- electrolyte. The slow recombination kinetics of the I^-/I_3^- electrolyte makes it a favourable choice in DSSCs.[4] However, the volatile nature of the organic solvent in the I^-/I_3^- electrolyte has been said to trigger a drop in performance, lowering the reliability of this cell architecture. Thus, efforts have moved towards replacing the I^-/I_3^- electrolyte with a solid or quasi-solid hole transport material, by methods such as spin-coating, heating, or gelation.[5–11] Deposition of solid hole conductors in DSSCs has often faced challenges such as incomplete coverage of the thick mesoporous TiO_2 network or the additional cost of the gelator.[11–14] In 2012, Freitag *et al.* reported a "zombie" cell architecture solid-state DSSC where they slowly dried the copper complex electrolyte of a liquid-state DSSC until it transformed into a solid hole conductor.[15] The present record efficiencies for solid-state DSSCs (PCE = 10.7–11.7%) have been achieved using this method.[16,17] Meanwhile, some groups have reported the use of solid electrolytes in DSSCs.[18–20] The term "solid electrolyte" would often refer to solid ionic conductors, but could be used interchangeably with the terms "hole transport material" or "hole conductor" in cases where the ion motion and hole hopping happen simultaneously.

According to Freitag *et al.*, the key to successfully achieving an efficient solid-state hole conductor with the "zombie" method relates to the amorphous state of the material.[15] This raises the question of what would happen with the conventional I^-/I_3^- electrolyte under a similar evaporation process. In fact, iodide species at high concentration are known to go through a Grotthuss mechanism as described below:[10,21,22]

$$I_3^- + I^- \rightarrow I^- - I_2 \ldots I^- \rightarrow I^- \ldots I_2 - I^- \rightarrow I^- + I_3^- \quad (1)$$

Here, the charge transfer occurs through hole hopping and bond exchange between the polyiodide species. The electrical conductivity of polyiodides has been previously studied by several groups.[10,22–25]

In this study, we report a solid-state DSSC that is fabricated by the "zombie" method (*i.e.* slow drying of the injected liquid electrolyte), except that the original electrolyte is a standard I^-/I_3^- electrolyte. We found that the liquid I^-/I_3^- electrolyte (Liq-I) turns into a solid polyiodide hole transport material (Ply-I) by simply exposing the Liq-I to ambient air. Our liquid-state I^-/I_3^- DSSC (Liq-I DSSC) has an architecture of FTO/compact-TiO_2 (c-TiO_2)/mesoporous-TiO_2 (m-TiO_2)/dye/Ply-I/Pt/FTO, where the anode and cathode are fixed to each other by sealing the edges with UV-curing glue without an additional spacer. Although the basic architecture follows that by Cao *et al.*,[26] this is the first report of a working glued DSSC employing an I^-/I_3^- electrolyte and Pt counter electrode, to the best of our knowledge. The organic 5T dye (Fig. 1)[27] was selected as the sensitizer for the following reasons: (1) the optimal film thickness (8 μm) is smaller than for other dyes such as N719 (20 μm),[28] greatly reducing the materials cost and cell fabrication time; (2) it revealed superior performance to other dyes tested in the solid-

School of Chemistry, The University of Edinburgh, David Brewster Road, Edinburgh EH9 3FJ, UK. E-mail: Neil.Robertson@ed.ac.uk

† Electronic supplementary information (ESI) available: Cell fabrication procedures; *JV*-curves; cell statistics; transient and light-soaking effects; XRD, Raman of polyiodide and precursors; FIB-SEM of cell; EIS. See DOI: 10.1039/d0ta07377f

Open Access Article. Published on 15 September 2020. Downloaded on 12/9/2025 1:00:59 AM.
This article is licensed under a Creative Commons Attribution-NonCommercial 3.0 Unported Licence.

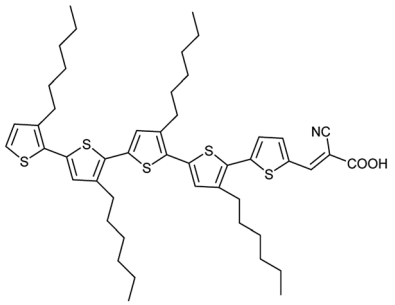

Fig. 1 Molecular representation of the 5T dye.

state DSSC structure adopted in this study; (3) its performance-cost ratio has been reported to be high.[29]

The unsealed DSSCs reached a maximum peak PCE of 5.2% (average 4.9%) and stabilized (stb.) PCE of 5.0% (average 3.6%). This indicates that our solid-state polyiodide DSSC (Ply-I DSSC) can reach a PCE almost as high as the corresponding precursor Liq-I DSSC (maximum peak PCE 5.7%, average 5.1%) and display excellent stability without leakage problems, with no loss in performance for a period around 10 months once a stabilization point is reached. This low-cost, simple, and versatile technique may expand the possibilities of forthcoming DSSC architectures.

Methods

Materials preparation

Reagents were purchased from Merck and used without further purification, unless otherwise specified. 5T dye was synthesized according to the literature.[27] 1,2-Dimethyl-3-propylimidazolium iodide (DMPII) was purchased from Solaronix and used without further purification. LiI was purchased from Fisher Scientific and used without further purification.

Fabrication of dye-sensitized solar cells (DSSCs)

Photoanodes. Fluorine-doped tin oxide (FTO) conductive glass (Merck, 7 Ω sq^{-1}) was pre-cut into 1.5 cm × 2.2 cm rectangles and cleaned by sonication in a 2% aqueous detergent solution (Hellmanex, Hellma), water and ethanol, followed by UV/O_3 treatment for 15 min. A compact TiO_2 layer was formed by immersing the substrate in 40 mM $TiCl_4$ aq. at 70 °C for 30 min. Commercial pastes, 30NR-D and WER2-O (Greatcell Solar), were screen-printed and annealed at 500 °C for 15 min to result in an 8 μm-thick TiO_2 film (4 μm transparent layer + 4 μm scattering layer) with a 0.2827 cm^2 (d = 6 mm) circular area. A $TiCl_4$ post-treatment was applied, followed by annealing at 500 °C for 30 min. The films were introduced in the dye bath while they were still warm (60–80 °C) and were left at r.t. overnight. The dye bath consisted of 0.1 mM 5T dye in ethanol/chloroform 7 : 3 (v/v) with 0.4 mM chenodeoxycholic acid.

Cathodes. FTO glass (1.5 cm × 2.2 cm) was cleaned in 0.1 M HCl/ethanol, ethanol and acetone. Platisol T/SP (Solaronix) was doctor-bladed on the substrate, followed by annealing at 400 °C for 15 min to obtain a platinized FTO glass electrode.

Assembly. The anode and cathode were assembled by clipping them directly face-to-face and sealing the edges with a UV-curing sealant (TB3035B, Threebond) and UV torch. The electrolyte was vacuum filled through a pre-drilled hole in the cathode and sealed with the UV-curing sealant. The composition of the electrolyte was 0.05 M I_2, 0.6 M 1,2-dimethyl-3-propylimidazolium iodide (DMPII), 0.1 M LiI and 0.5 M 4-*tert*-butylpyridine (*t*BP) in acetonitrile (MeCN). The seal was opened after 2 days to obtain the solid-state cells.

Variations of the above procedures involving different dyes and spacers are detailed in the ESI.†

Characterization methods

UV-Vis absorption was recorded on a V-670 (Jasco) spectrophotometer. Each sample was placed and sealed between two pieces of microscope glass (=cell). The reference was a blank cell without any sample inside. Photocurrent–voltage (J–V) curves were recorded on an Autolab potentiostat (Metrohm) with class AAA SLB300A solar simulator (Sciencetech) as the light source. The light intensity was calibrated to AM1.5G using a silicon reference cell. The active area of the solar cell was fixed with a black metal mask, either with a circular aperture of 0.126 cm^2 (d = 4 mm) or a square aperture of 0.0625 cm^2 (2.5 mm × 2.5 mm). The frequency-modulated electrochemical impedance was recorded with a similar setup to that of the J–V measurements. The frequency range was set to 100 kHz to 100 mHz with an AC voltage amplitude of 10 mV. The measurements were performed at open circuit voltage under 1 sun illumination. The plots were fitted using the ZView (Scribner Associates) software. Incident photon-to-current conversion efficiency (IPCE) was recorded with a Bentham PVE300 EQE/IQE system in DC mode. The incident light was calibrated with a reference silicon photodiode within the range of 300–1000 nm. Raman spectra were recorded on an inVia Renishaw micro Raman spectrometer. Fourier-transform infrared (FT-IR) spectra were recorded on a Shimadzu IRSpirit FT-IR spectrophotometer at attenuated total reflection mode. Focused ion beam scanning electron microscopy (FIB-SEM) images were taken on a Zeiss Crossbeam 550 FIB-SEM. The sample was sputtered with platinum prior to the measurement and the cross-section was captured at a 36° angle. Energy dispersive X-ray spectroscopy analysis was performed on an X-Max 150 EDS detector (Oxford Instruments) with a detector size of 150 mm^2.

Results and discussion

Performance and stability of Ply-I DSSC

According to our trials, Ply-I DSSCs can be fabricated with a wide choice of components such as different dyes (*e.g.* N719, SQ2, 5T, D149) and spacers (*e.g.* thermal polymer spacer, UV-curing glue) (Fig. S1†). The results indicate that the basic effect can be widely adapted to such variations. Although none of the dyes above have been optimised, the relatively high performance achieved with 5T dye could be related to properties such as relatively thin film thickness and efficient light harvesting. Detailed study was focused on the architecture FTO/c-

 This journal is © The Royal Society of Chemistry 2020

Open Access Article. Published on 15 September 2020. Downloaded on 12/9/2025 1:00:59 AM.
This article is licensed under a Creative Commons Attribution-NonCommercial 3.0 Unported Licence.

TiO_2/m-TiO_2/5T-dye/Ply-I/Pt with which the highest PCEs were achieved. To simplify device fabrication, the electrodes were attached without a spacer but by applying UV-curing glue along the edges of the assembly. Fig. 2 shows *J–V* curves of the Liq-I DSSC with the best PCE (Cell 1), Ply-I DSSC with the best "peak PCE" (Ply-I (peak)) (Cell 1), Ply-I DSSC with the best "stabilized PCE" (Ply-I (stb.)) (Cell 2) at 1500 h and best Ply-I (stb.) DSSC (Cell 2) at 8000 h. The overall photovoltaic parameters (short-circuit photocurrent density (J_{SC}), open-circuit voltage (V_{OC}), fill factor (ff) and PCE) of the Liq-I DSSC, Ply-I (peak) DSSC and Ply-I (stb.) DSSC are summarized in Table 1 and Fig. S2.† The *J–V* curves of the best Ply-I (stb.) DSSC measured with a 0.0625 cm^2 aperture at 0 h (Liq-I), Ply-I (peak), 1500 h and 8000 h can be found in the ESI (Fig. S3).† With a 0.0625 cm^2 aperture, the best Ply-I (peak) DSSC achieved J_{SC} = 10.8 mA cm^{-2}, V_{OC} = 0.70 V, ff = 0.71 and PCE = 5.3%. The best Ply-I (stb.) DSSC achieved J_{SC} = 10.3 mA cm^{-2}, V_{OC} = 0.63 V, ff = 0.69 and PCE = 4.5% after 1500 h, and J_{SC} = 11.3 mA cm^{-2}, V_{OC} = 0.66 V, ff = 0.67 and PCE = 5.0% after 8000 h. In general, the performance trends by comparing the two masks were analogous to what has previously been reported by Ito *et al.*[30] In summary, slightly higher PCE and more consistent results are obtained with the 0.0625 cm^2 aperture, while results with larger active area will be obtained with the 0.126 cm^2 aperture. The two masks were used in this study to validate the obtained results. Once the DSSCs are unsealed, the photovoltaic parameters evolve as depicted in Fig. 3 (stability-test protocol ISOS-D-1).[31] Once unsealed, the solid-state characteristics (*i.e.* shrinkage of excess electrolyte, S-shape observed in *J–V* curve) will start to appear after a few days, however the performance tends to fluctuate for each point of measurement within the first several hundred hours counting from T = 0. The Ply-I DSSCs will eventually reach a stabilization point where the DSSC performance becomes stable. We note that the timeline above is approximate and the evolution speed towards Ply-I (stb.) differs from cell to cell. Clearer descriptions are expected to be provided once the best protocol is fully optimized.

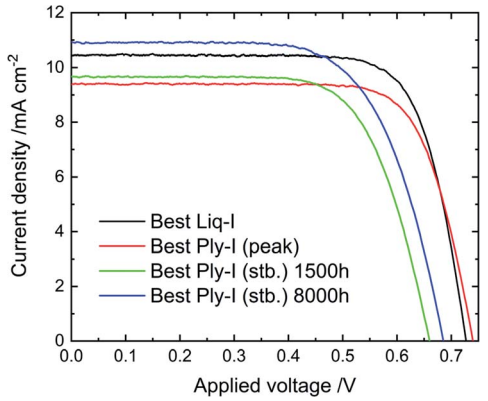

Fig. 2 *J–V* curves of DSSCs using 5T dye with an aperture of 0.126 cm^2. Black: best Liq-I DSSC (Cell 1). Red: best Ply-I (peak) DSSC, obtained by drying Cell 1. Green: best Ply-I (stb.) (Cell 2) DSSC measured after 1500 h. Blue: best Ply-I (stb.) DSSC (Cell 2) measured after 8000 h. The Liq-I DSSC is sealed and the Ply-I DSSCs are unsealed.

In general, a decrease in ff and J_{SC} contribute to an eventual drop in PCE. The V_{OC}, however, initially rises and only drops slightly thereafter in most cases. The Ply-I DSSC with the highest stb. PCE was tracked further for 3–4 months, revealing excellent stability (Fig. 3). During this period (T = 1000–3200 h), the unsealed DSSC exhibited PCE values in the range of 4.0 ± 0.2% with a 0.126 cm^2 aperture and 4.6 ± 0.2% with a 0.0625 cm^2 aperture. The lifetime of the cell was estimated by linearly fitting the plots, returning T_{80} (time until 20% PCE drop from T = 0 h in Fig. 3(d))[31] as 4516 h and 14 544 h with apertures of 0.126 cm^2 and 0.0625 cm^2, respectively. The T_{S80} (time until 20% PCE drop from the stabilized onset in Fig. 3(d); T = 1008 h for 0.126 cm^2 and T = 600 h for 0.0625 cm^2) values were 4315 h and 14 344 h, respectively. The calculations are explained in detail in the ESI (Fig. S4†). T_{S80} in the optimum case (=14 344 h) indicates a lifetime of 1.6 years counting from T = 600 h in Fig. 3(d). In other words, the fitted curves suggest that 0.196% PCE (0.126 cm^2) or 0.065% PCE (0.0625 cm^2) in absolute values is lost every 1000 h. To validate our estimation, the same unsealed Ply-I DSSC was measured after another several months, revealing no loss in performance for the entire 9–10 months, or ~7000 h, counting from T = 1008 h. In Fig. 3(a) and (d), the J_{SC} and PCE appear to have improved during the dark storage for 5000 h. We are not certain at this point if the improvement is within the deviation error, or if the dark storage has any effect to improve the device performance. For reference, the performance after a week (the last plot, 8112 h) shows a slight decrease in performance, but still higher than the previous plots. Although the results may not represent real-life operational stability, such a long shelf lifetime is rarely reported in DSSCs to the best of our knowledge. The corrosiveness of I^-/I_3^-, one of the main issues of concern for a Liq-I DSSC,[4,5] appears to be less of a problem in the Ply-I DSSC.

Photo-response of Ply-I

The forward *J–V* scan of a Ply-I DSSC stored in the dark depicts a characteristic S-shape, which gradually disappears upon light soaking (Fig. 4(a)). Each *J–V* curve in Fig. 4(a) is scanned in the order J_{SC} → V_{OC} → J_{SC}, revealing the dynamic *J–V* response to light. The dynamics appears to be purely photo-responsive and not bias-related (Fig. S5†). Similar S-shape *J–V* dynamics have been observed in organic solar cells, where the authors attributed the light soaking effect to the reduction of charge transport resistance in the TiO_x electron transport layer.[32] In our case, the S-shape profile is likely to come from the Ply-I layer. The drop from peak current to steady-state current can be explained by the imbalance between the number of photogenerated charges from the sensitized-TiO_2 and mobile charges in the mass transport limited Ply-I.[33]

The transient *J–V* behaviour of the Ply-I DSSC was tracked for 20 min under continuous light soaking as shown in Fig. 4(b) (stability-test protocol ISOS-L-1).[31] The J_{SC}, ff and PCE rise whereas the V_{OC} declines, with all parameters reaching an equilibrium after 5–10 min illumination. Interestingly, the initial S-shape was more noticeable when a smaller mask (*e.g.* 0.0625 cm^2) was used as an aperture. In addition, when the

Open Access Article. Published on 15 September 2020. Downloaded on 12/9/2025 1:00:59 AM.
This article is licensed under a Creative Commons Attribution-NonCommercial 3.0 Unported Licence.

Table 1 Photovoltaic parameters of the best Liq-I DSSC, Ply-I (peak) DSSC and Ply-I (stb.) DSSC measured with a 0.126 cm^2 aperture. The values in brackets are the average of four to seven cells each

	J_{SC}/mA cm^{-2}	V_{OC}/V	ff	PCE (%)
Liq-I best	10.4	0.73	0.75	5.7
Liq-I average	(9.7 ± 1.2)	(0.71 ± 0.02)	(0.73 ± 0.04)	(5.1 ± 0.8)
Ply-I (peak)	9.38	0.74	0.75	5.2
Ply-I (peak) average	(9.3 ± 1.4)	(0.73 ± 0.01)	(0.71 ± 0.04)	(4.9 ± 0.6)
Ply-I (stb.) 1500 h	9.69	0.66	0.69	4.4
Ply-I (stb.) 8000 h	10.9	0.69	0.66	5.0
Ply-I (stb.) average[a]	(8.5 ± 1.7)	(0.68 ± 0.04)	(0.63 ± 0.07)	(3.6 ± 0.7)

[a] Liq-I average: from the performance of individual cells before unsealing. Ply-I (peak) average: from the best performance of individual cells within the non-stabilized region; from the point the cell has started to show Ply-I characteristics such as S-shape *J–V* curve and darkening of the electrolyte, and before reaching the stabilized performance. The approximate time range was between 24 to several hundred hours. Ply (stb.) average: from the best performance of individual cells within the stabilized region, typically from 48 to 750 h (the value for the best cell was taken from the measurement at 8000 h).

mask was lifted after several minutes of irradiation, a silhouette of the masked area appeared on the surface of the active area, covering the area where the aperture had been. (Fig. S6†). Once formed, the silhouette is observable for *ca.* half an hour. The dynamic *J–V* characteristics and darkening of the illuminated area resonate with each other. The darkening may be related to partial photooxidation of the iodide species.[4] Acceleration in oxidation and release of charges in response to light would enhance charge transport, thus increasing the current and ff.

IPCE was recorded to investigate the monochromatic response of Ply-I (Fig. 5(a)). The IPCE exceeds 70% around 500 nm. The dip around 360 nm overlaps with the optical absorption peak of the Ply-I (Fig. 5(b)), suggesting that light absorption by the Ply-I might be one of the causes of the slightly lower current in the Ply-I DSSC. We note that Ply-I itself acts as a DSSC light absorber, albeit very inefficiently with J_{SC} = 80 μA cm^{-2} and V_{OC} = 0.24 V (Fig. S7†). The much higher and broader absorption by Ply-I is coherent with its darker colour compared to Liq-I. The optical gaps were calculated as 2.64 eV for Liq-I and 2.39 eV for Ply-I. The corresponding Tauc plots are shown in Fig. S8.† The broadening of the main IPCE peak towards longer wavelengths in the case of Ply-I DSSC could be due to some interface modification between the TiO_2 and Ply-I.

Formation of Ply-I

Ply-I is sparsely soluble in water and soluble in organic solvents such as ethanol and acetone. The layer is amorphous as

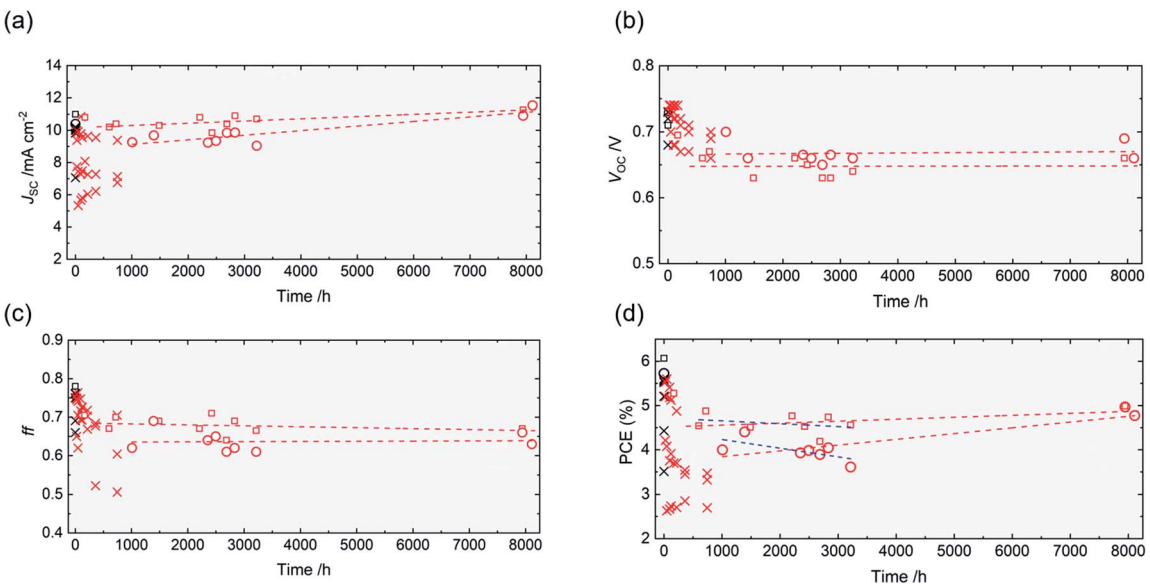

Fig. 3 (a)–(d) Evolution of the photovoltaic parameters of Ply-I DSSCs for ~8000 h. The performance of the best Ply-I (stb.) DSSC was tracked for 8000 h, while the other cells were tracked for 750 h. Black plots: sealed Liq-I DSSCs. Red plots: unsealed Ply-I DSSCs. Crosses indicate individual DSSCs measured with an aperture of 0.126 cm^2. Black open circles indicate the best Liq-I DSSC, measured with an aperture of 0.126 cm^2. Red open circles indicate the long-term evolution of the best Ply-I (stb.) DSSC, measured with an aperture of 0.126 cm^2. Red open squares indicate the long-term evolution of the same DSSC (with the best stb. PCE), measured with an aperture of 0.0625 cm^2. The red dashed lines are the linear fitting of the red squares and circles in the stabilized region from 1000 h to 8000 h, presented as a guide to the eye. The blue dashed lines in Fig. 3(d) are the linear fittings of the red circles and red squares in the stabilized region up to 3200 h.

 This journal is © The Royal Society of Chemistry 2020

Open Access Article. Published on 15 September 2020. Downloaded on 12/9/2025 1:00:59 AM.
This article is licensed under a Creative Commons Attribution-NonCommercial 3.0 Unported Licence.

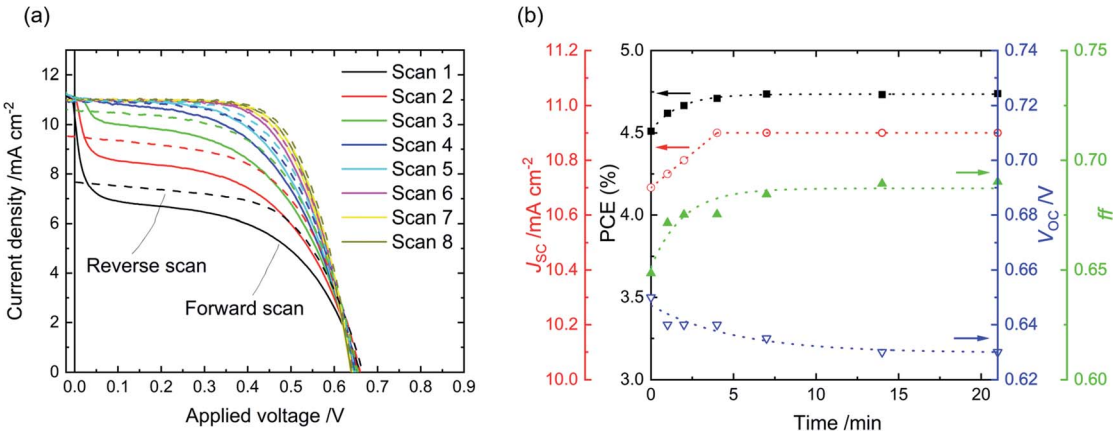

Fig. 4 (a) Successive J–V scans of a Ply-I DSSC at 100 mW cm^{-2} after dark storage. Solid line: forward scan. Dashed line: reverse scan. A 0.0625 cm^2 aperture was used. The distinct S-shape eventually disappears after multiple scans under 1 sun illumination. (b) Tracked performance of a Ply-I DSSC for 20 min under constant 1 sun illumination. Each value is from an independent scan.

confirmed by XRD (Fig. S9†), which is consistent with the solar cell characteristics we have described.[15]

The Raman spectra of Liq-I and Ply-I in Fig. 6(a) both show a sharp peak at 112 cm^{-1} and a shoulder at 115 cm^{-2}. The former corresponds to I_3^- (ref. 10 and 34) and the latter to $I_2^{-\bullet}$.[35] Ply-I has a prominent additional peak at 149 cm^{-1}, which can be assigned to I_5^-.[10,24,36,37] Neither of the samples have signs of free-standing molecular I_2 (~180 cm^{-1}), but the small peak at 174 cm^{-1} found in Ply-I suggests the existence of adsorbed iodine.[38] The absence of molecular I_2 in the Ply-I indicates that most of the I_2 has been consumed to form higher order polyiodides. The Liq-I components are DMPII, LiI, I_2, *t*BP and MeCN (Fig. S10(a)†). The creation of polyiodide from iodide species is further investigated in Fig. 6(b), where the two characteristic peaks at 112 cm^{-1} and 149 cm^{-1} appear with, and only with, the combination of DMPII + I_2 and LiI + I_2 (the Raman spectra of *t*BP and MeCN are shown in Fig. S10(b)†).

We would like to note that the peak at 149 cm^{-1} is more intense for I_2 + LiI than for I_2 + DMPII. This suggests that LiI is more likely to facilitate the intermolecular bonding of the iodide species, probably due to the Li^+ being small.

The visual appearance is also different; I_2 + LiI develops an intense dark brown colour compared to I_2 + DMPII. The intense colour is likely to correspond to the formation of higher order polyiodides. As the colour gradually fades away, the Raman peaks associated with polyiodides also diminish, indicating that I_2 dissociates from the structure by evaporating into the air (Fig. S11†).

We investigated the formation of Ply-I in further detail by placing drops of I_2/MeCN, LiI + I_2/MeCN and Liq-I on a glass slide as shown in Video S1.† The concentrations were identical as in a normal electrolyte. The I_2/MeCN displays a yellow orange colour, which evaporates after a couple of minutes. LiI + I_2/MeCN dramatically changes from yellow brown to dark brown over a minute, followed by disappearance of the colour. White LiI crystals remain in the end. The Liq-I slightly darkens over a minute from yellow to orange and maintains its colour thereafter. We summarize our observation as follows.

(1) As the MeCN evaporates, the I^-, I_3^- and I_2 react to form higher order polyiodides (intensification of brown colour). (2) Without the *t*BP, the polyiodides are not stable and decompose into LiI (or DMPII) and I_2. The I_2 will eventually sublime. (3) In the presence of *t*BP, the polyiodide is stable for weeks. It is

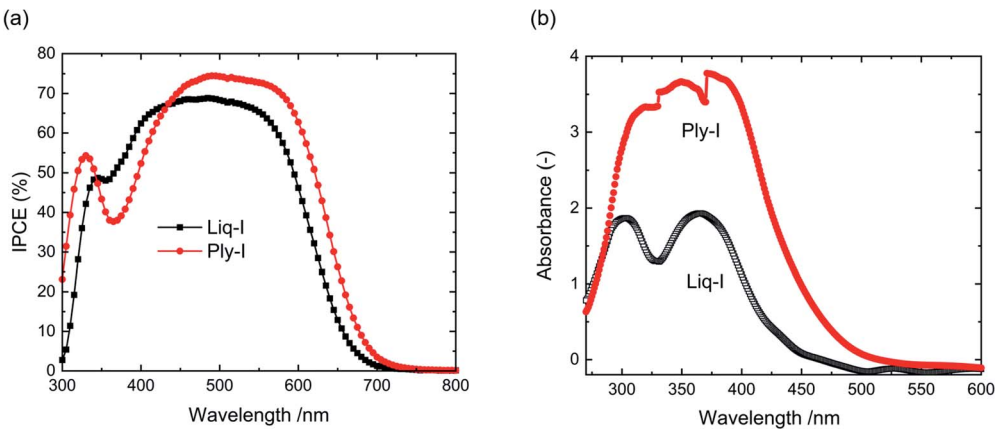

Fig. 5 (a) IPCE curve of Liq-I DSSC and Ply-I DSSC. (b) UV-Vis absorption spectra of Liq-I and Ply-I.

Open Access Article. Published on 15 September 2020. Downloaded on 12/9/2025 1:00:59 AM.
This article is licensed under a Creative Commons Attribution-NonCommercial 3.0 Unported Licence.

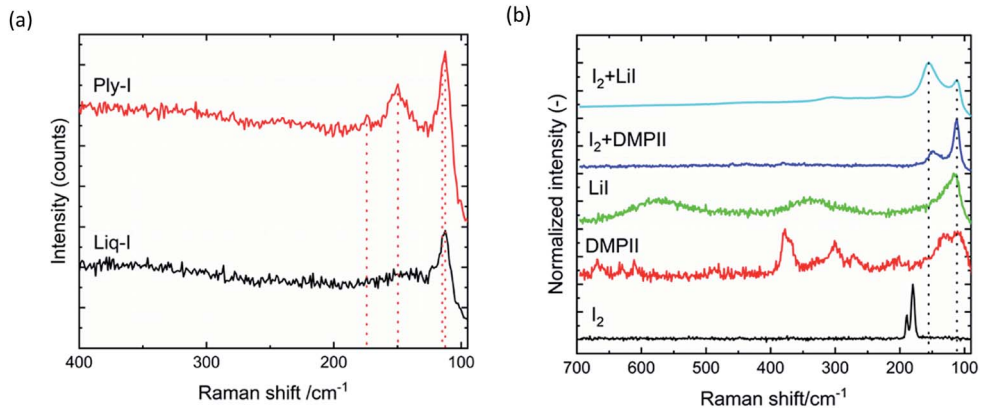

Fig. 6 (a) Raman spectra of Ply-I and Liq-I. (b) Raman spectra of LiI + I_2, DMPII + I_2, LiI, DMPII and I_2 solid samples.

possible that the *t*BP acts as a Lewis base and forms a complex with the LiI (or DMPII) or I_2 to fix the polyiodide network.[24,39]

To note, the above observations were identical in the dark. This indicates that the polyiodide can form without the presence of light.

Is Ply-I solvent-free?

The IR spectra in Fig. 7 can give further indications on the properties of Ply-I. A full assignment of the peaks can be found in the Table S2.† The absence of the –C≡N peak at 2250 cm^{-1} in the Ply-I spectrum indicates that Ply-I is free of MeCN. The peak appears in the Liq-I spectrum. Traces peaks of MeCN are also identified in the DMPIII + I_2 and LiI + I_2, due to the preparation of these samples taking place just before the IR measurement. On the other hand, a broad distinctive peak at 3200–3600 cm^{-1} is seen in Ply-I, DMPII + I_2 and LiI + I_2. The peak can be assigned to the –OH stretching in water molecules. The water was likely adsorbed from the air during the measurement, as DMPII and LiI are both hygroscopic. In fact, the DMPII and LiI spectra in Fig. 7(b) show only the peaks assigned to water. However, additional peaks associated to C–H bonding appear especially when DMPII is reacted with I_2 (Fig. 7(a)). These new peaks are reflected in the Ply-I. The appearance of new peaks by simply mixing the raw ingredients may be an indication that the water uptake is lower in the Ply-I compared to the raw DMPII and LiI. Although solid conclusions cannot be drawn at this point due to the lack of quantitative interpretation, the stability of the Ply-I indicates its low sensitivity to atmospheric moisture. The Ply-I cells differ from aqueous I^-/I_3^- DSSCs in which the I^-/I_3^- species are dissolved in water.[40,41]

Ply-I network in the DSSC

The cross-section FIB-SEM image of an opened Ply-I DSSC is shown in Fig. S12.† Iodine is observed throughout from the top surface to the vicinity of the FTO layer in the energy dispersive X-ray spectroscopy image. The image confirms that the Ply-I is evenly distributed in the sensitized-TiO_2 mesoporous network to allow optimal performance. From the above finding, we propose the schematic architecture of Liq-I and Ply-I DSSC as in Fig. 8. In addition to the suggested model by Cao *et al.*,[26] we

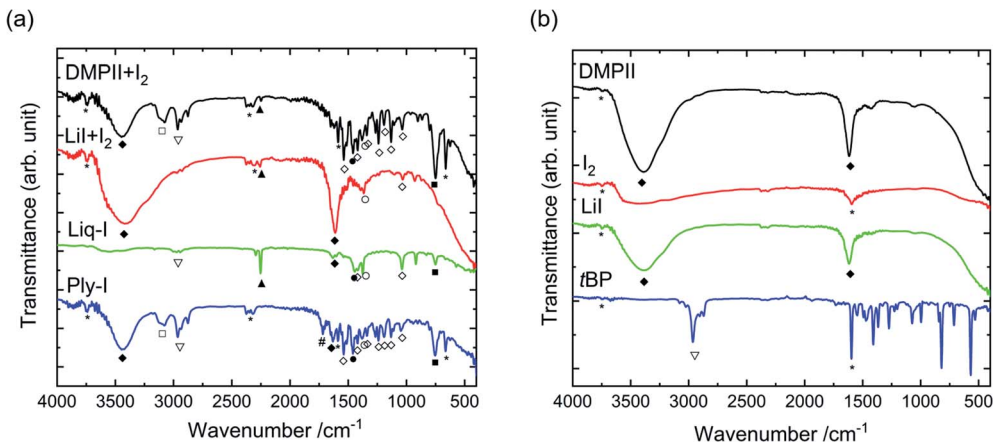

Fig. 7 IR spectra of (a) DMPII + I_2, LiI + I_2, Liq-I, Ply-I and (b) DMPII, I_2, LiI, and *t*BP. The peak assignments are listed in Table S2.† For the samples DMPII + I_2 and LiI + I_2, 0.6 M DMPII (or 0.1 M LiI) and 0.05 M I_2 in MeCN was placed on the IR instrument and dried on place before the measurement.

 This journal is © The Royal Society of Chemistry 2020

Open Access Article. Published on 15 September 2020. Downloaded on 12/9/2025 1:00:59 AM.
This article is licensed under a Creative Commons Attribution-NonCommercial 3.0 Unported Licence.

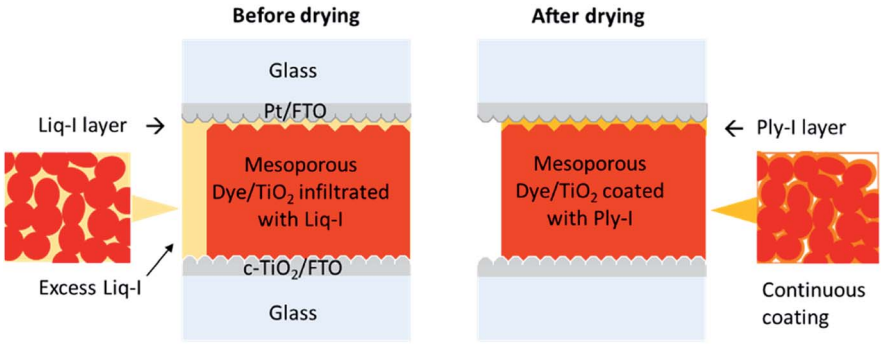

Fig. 8 Schematic cross-section model of the Liq-I DSSC and Ply-I DSSC fabricated in this study.

observe a recognisable thin layer of Liq-I or Ply-I between the counter electrode and dye-sensitized TiO_2 (Fig. S13(a)†). *J–V* measurements of an assembled cell before injecting the electrolyte revealed that the Pt/FTO electrode and sensitized TiO_2 are in weak but negligible contact, indicating the existence of a narrow gap (Fig. S13(b)†). The Liq-I (or Ply-I) can infiltrate this gap and prevent electrical shunting during the operation of the cell. Our result appears to be different from the outcomes in previous studies; the fact that the Pt cathode worked in the spacer-free architecture might be related to the softer pressure applied to the electrodes during the assembly of the cell.[26,33]

Another fact that needs to be considered is why Ply-I DSSCs are functional while the normal belief is that I^-/I_3^- liquid-state DSSCs will stop operating once the electrolyte has dried out. The difference, we believe, should be related to the controllability of the electrolyte drying process (*i.e.* route and speed).

Uncontrolled drying will often cause the electrolyte to dry out in a manner whereby the solid species would not remain between the cathode and the sensitized-TiO_2 to bridge the charges. For instance, the Liq-I injection hole should be placed in an appropriate position such that the solvent is drawn towards the active area, letting the solid species cover the mesoporous network instead of going to the edges of the glass. In our case, the hole was positioned near the boundary of the active area. If the excess Liq-I species, initially located outside the active area, accumulate on top of the mesoporous network during the drying process then this may prevent the generation of voids caused by the shrinkage of the Liq-I to a minimum. An example of a DSSC before and after drying is shown in Fig.-S13(c).† The drying speed may also matter. Accelerated drying of the Liq-I by heating at 50 °C or simply leaving it exposed to ambient air results in a gel with a dark yellow colour that resembles the Ply-I. However, Raman spectra revealed that less higher-order polyiodides are present in these gels (Fig. S14†). Accelerated drying also tends to initiate unwanted aggregation, cracks or voids, increasing the number of grain boundaries or discontinuous interfaces that would contribute to higher charge transport resistance. Within the mesoporous TiO_2 film, a thin continuous amorphous coating of Ply-I should suffice for efficient charge transport by the Grotthuss mechanism. Slow drying is likely to facilitate the formation of such a layer, analogous to the findings by Freitag *et al.*[15]

Charge transport properties in the Ply-I DSSC

The mechanism of the Ply-I DSSC was further investigated by electrochemical impedance spectroscopy. Fig. 9 shows the Nyquist plots at 1 sun for the Liq-I DSSC, Ply-I (peak) DSSC and Ply-I (stb.) DSSC. The Bode phase and magnitude plots are described in Fig. S15.† There are two noticeable semicircles in the Nyquist plots, where the one at higher frequencies ($Z' \sim 20$–$30\ \Omega$) (Region 1) is associated with the Pt/Ply-I (or Pt/Liq-I) interface, while the one at lower frequencies ($Z' > 30\ \Omega$) (Region 2) is associated with the TiO_2/Ply-I (or TiO_2/Liq-I) interface. No distinct semicircles assignable to the *RC* element of the Ply-I (or Nernst-diffusion of the Liq-I) (Region 3) were identified in the plotted curves. The absence of this region in the Nyquist plot has been reported for a glue-based Cu^+/Cu^{2+} electrolyte DSSC, where the authors related the phenomenon to the reduced thickness of the electrolyte layer compared to a DSSC using a μm-thick spacer.[26] We assume that the same theory can be applied to our glue-based Liq-I DSSCs and Ply-I DSSCs. The phenomenon demonstrates the efficient charge transport and regeneration in Ply-I.

Based on our observations, the plots were fitted using the equivalent circuit shown in Fig. S16.† The model was constructed based on a simplified circuit proposed by Cao *et al.*[42] For the Liq-I DSSC and Ply-I (peak) DSSC, an additional LR_{rec2} element was placed in parallel with the $R_{rec}C_{\mu}$ element to match

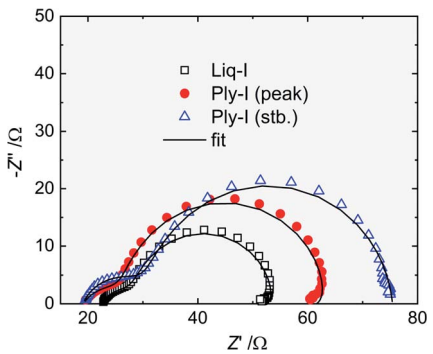

Fig. 9 Nyquist plots of the Liq-I DSSC and Ply-I DSSC under 1 sun illumination. The solid lines are the fitted curves using the equivalent circuit in Fig. S16.†

Open Access Article. Published on 15 September 2020. Downloaded on 12/9/2025 1:00:59 AM.
This article is licensed under a Creative Commons Attribution-NonCommercial 3.0 Unported Licence.

Table 2 Summary of values obtained from the electrochemical impedance fitting. R_{Pt}: resistance at Pt/Ply-I (or Liq-I); C_{Pt}: capacitance at Pt/Ply-I (or Liq-I); R_{rec}: recombination resistance; C_{μ}: chemical capacitance; τ_e: electron lifetime

	Liq-I	Ply-I (peak)	Ply-I (stb.)
R_{Pt} [Ω]	6.65	7.90	12.1
C_{Pt} [μF]	13.0	12.0	7.21
R_{rec} [Ω]	25.0	36.6	44.3
C_{μ} [μF]	173	184	182
τ_e [ms]	4.32	6.73	8.06

the inductive loop observed at the tail of the Nyquist plots (<~1 Hz). Appearance of this loop in a solar cell at forward bias and low frequency is an indication of an additional recombination pathway from the TiO_2 to the other layers.[43] In our case, this could be the recombination between the dye/TiO_2 and Pt cathode, as supported by the very weak photocurrent arising in the DSSC in the absence of the electrolyte (Fig. S13†). It is interesting to note, however, that the inductive behaviour disappears once the Ply-I DSSC is stabilized. This suggests that some modification of the interfaces has occurred through the evolvement from Liq-I to Ply-I.

The values from the fitting are summarized in Table 2. The rise in R_{Pt} from Liq-I to Ply-I may be due to the slightly poorer attachment of Ply-I to the Pt/FTO counter electrode due to pinholes created during the evaporation of the solvent. Extra resistance at this interface can slow the dye regeneration thus lower the ff and J_{SC}. Optimising the drying process (*e.g.* speed) should improve these parameters. The electron lifetime (τ_e) of the TiO_2 conduction band electrons was estimated from the fitted R_{rec} and C_{μ} values, *i.e.* $\tau_e = R_{rec} \times C_{\mu}$. The electron lifetime extends from Liq-I to Ply-I, mainly due to the rise in R_{rec}. The trend explains the increase in V_{OC} from Liq-I to Ply-I (peak). The slight V_{OC} drop to Ply-I (stb.), however, suggests that either the TiO_2 conduction band edge or the HOMO of the Ply-I (or redox potential of Liq-I) has shifted towards lowering the V_{OC}. It is likely that the potential of Ply-I has shifted towards higher energy due to the stronger intermolecular interactions in the solid-state. This is supported by the narrower optical gap observed for Ply-I compared to Liq-I as described earlier. In summary, the increase in R_{Pt} leads to lower J_{SC} and ff, while the extended electron lifetime and change in energy alignment lead to small fluctuations of the V_{OC}, keeping it a rather constant value overall.

Conclusions

In this study, we challenged the common belief that a standard I^-/I_3^- DSSC will stop operating once the electrolyte has "dried out." Solid-state DSSCs with good efficiency and excellent stability were obtained when the electrolyte solvent of a I^-/I_3^- cell was slowly evaporated in a controlled manner. The as-prepared solid hole conductor (Ply-I) was confirmed to have different properties from the liquid electrolyte (Liq-I) such as higher optical absorption, dynamic photo-responsive *J–V* characteristics, and higher order polyiodides in the structure. From the dark-storage stability tests, the Ply-I DSSC was found to have no loss in performance for a period up to 10 months totally unsealed, suggesting that it may operate for a sufficiently long time in real-life conditions with proper encapsulation. The Ply-I DSSC with 5T dye can reach a maximum peak PCE = 5.2% and stabilized PCE = 5.0%, close to the corresponding standard Liq-I DSSC with maximum PCE = 5.7%, but with higher stability. Although the protocol to achieve high performance Ply-I cells with good reproducibility is yet to be optimized, the simplicity of the materials and methods used to obtain these cells, along with the peculiar characteristics they display should provoke high scientific interest. Studies on further device optimization and comprehension of the operation mechanism may lead the DSSC field to new horizons. Some important future directions include investigation on the optimal amount of iodine in the precursor Liq-I, as well as to conclude whether the adsorbed water from the air has any influence on the performance of the Ply-I DSSC.

Conflicts of interest

There are no conflicts to declare.

Acknowledgements

The authors acknowledge the Centre for Plastic Electronics (CPE) access to their IPCE facility. The authors thank Dr M. Planells for providing the 5T dye and Dr A. Gromov for providing access to the Raman spectroscopy instrument. The authors acknowledge the use of the FIB-SEM bought with the EPSRC grant EP/P030564/1 and Dr Thomas Glen for help with the image acquisition. ET thanks S. Hunter and Dr H. Benjamin for the assistance and helpful discussions for some of the work presented in the study. ET acknowledges JASSO for a PhD studentship. Finally, the authors are grateful to the reviewers for their insights and discussions on the original manuscript.

References

1 H. Gerischer, M. E. Michel-Beyerle, F. Rebentrost and H. Tributsch, *Electrochim. Acta*, 1968, **13**, 1509–1515.
2 H. Tsubomura, M. Matsumura, Y. Nomura and T. Amamiya, *Nature*, 1976, **261**, 402–403.
3 B. O'Regan and M. Grätzel, *Nature*, 1991, **353**, 737–740.
4 G. Boschloo and A. Hagfeldt, *Acc. Chem. Res.*, 2009, **42**, 1819–1826.
5 J. Wu, Z. Lan, J. Lin, M. Huang, Y. Huang, L. Fan and G. Luo, *Chem. Rev.*, 2015, **115**, 2136–2173.
6 L. Schmidt-mende, U. Bach, R. Humphry-baker, T. Horiuchi, H. Miura, S. Ito, S. Uchida and M. Grätzel, *Adv. Mater.*, 2005, **17**, 813–815.
7 N. Kato, S. Moribe, M. Shiozawa, R. Suzuki, K. Higuchi, A. Suzuki, M. Sreenivasu, K. Tsuchimoto, K. Tatematsu, K. Mizumoto, S. Doi and T. Toyoda, *J. Mater. Chem. A*, 2018, **6**, 22508–22512.

 This journal is © The Royal Society of Chemistry 2020

Open Access Article. Published on 15 September 2020. Downloaded on 12/9/2025 1:00:59 AM.
This article is licensed under a Creative Commons Attribution-NonCommercial 3.0 Unported Licence.

8 P. Liu, B. Xu, K. M. Karlsson, J. Zhang, N. Vlachopoulos, G. Boschloo, L. Sun and L. Kloo, *J. Mater. Chem. A*, 2015, **3**, 4420–4427.
9 S.-H. Park, J. Lim, I. Y. Song, J.-R. Lee and T. Park, *Adv. Energy Mater.*, 2014, **4**, 1300489.
10 W. Kubo, K. Murakoshi, T. Kitamura, S. Yoshida, M. Haruki, K. Hanabusa, H. Shirai, Y. Wada and S. Yanagida, *J. Phys. Chem. B*, 2001, **105**, 12809–12815.
11 J. T. Park, W. S. Chi, D. K. Roh, S. H. Ahn and J. H. Kim, *Adv. Funct. Mater.*, 2013, **23**, 26–33.
12 J. E. Kroeze, N. Hirata, L. Schmidt-mende, C. Orizu, S. D. Ogier, K. Carr, M. Grätzel and J. R. Durrant, *Adv. Funct. Mater.*, 2006, **16**, 1832–1838.
13 L. Schmidt-Mende and M. Grätzel, *Thin Solid Films*, 2006, **500**, 296–301.
14 Z. Huo, L. Wang, L. Tao, Y. Ding, J. Yi, A. Alsaedi, T. Hayat and S. Dai, *J. Power Sources*, 2017, **359**, 80–87.
15 M. Freitag, Q. Daniel, M. Pazoki, K. Sveinbjörnsson, J. Zhang, L. Sun, A. Hagfeldt and G. Boschloo, *Energy Environ. Sci.*, 2015, **8**, 2634–2637.
16 W. Zhang, Y. Wu, H. W. Bahng, Y. Cao, C. Yi, Y. Saygili, J. Luo, Y. Liu, L. Kavan, J. E. Moser, A. Hagfeldt, H. Tian, S. M. Zakeeruddin, W.-H. Zhu and M. Grätzel, *Energy Environ. Sci.*, 2018, **11**, 1779–1787.
17 H. Michaels, M. Rinderle, R. Freitag, I. Benesperi, T. Edvinsson, R. Socher, A. Gagliardi and M. Freitag, *Chem. Sci.*, 2020, **11**, 2895–2906.
18 T. He, Y. F. Wang and J. H. Zeng, *ACS Appl. Mater. Interfaces*, 2015, **7**, 21381–21390.
19 J. V. Vaghasiya, K. K. Sonigara, J. Prasad, T. Beuvier, A. Gibaud and S. S. Soni, *J. Mater. Chem. A*, 2017, **5**, 5373–5382.
20 P. Liu, J. M. Gardner and L. Kloo, *Chem. Commun.*, 2015, **51**, 14660–14662.
21 N. Agmon, *Chem. Phys. Lett.*, 1995, **244**, 456–462.
22 N. Papageorgiou, Y. Athanassov, M. Armand, P. Bonhôte, H. Pettersson, A. Azam and M. Grätzel, *J. Electrochem. Soc.*, 1996, **143**, 3099–3108.
23 M. A. Petit, A. H. Soum, M. Leclerc and R. E. Prud'Homme, *J. Polym. Sci.*, 1987, **25**, 423–433.
24 H. Yu, L. Yan, Y. He, H. Meng and W. Huang, *Chem. Commun.*, 2017, **53**, 432–435.
25 P. Tomasz, M. Ernst, D. Zimmer, P. Macchi and N. Casati, *Angew. Chem., Int. Ed.*, 2019, **58**, 6625–6629.
26 Y. Cao, Y. Liu, M. Zakeeruddin, A. Hagfeldt and M. Grätzel, *Joule*, 2018, **2**, 1108–1117.
27 M. Planells, A. Abate, H. J. Snaith and N. Robertson, *ACS Appl. Mater. Interfaces*, 2014, **6**, 17226–17235.
28 S. Ito, T. N. Murakami, P. Comte, P. Liska, C. Grätzel, M. K. Nazeeruddin and M. Grätzel, *Thin Solid Films*, 2008, **516**, 4613–4619.
29 E. Tanaka, H. Michaels, M. Freitag and N. Robertson, *J. Mater. Chem. A*, 2020, **8**, 1279–1287.
30 S. Ito, M. K. Nazeeruddin, P. Liska, P. Comte, R. Charvet, P. Péchy, M. Jirousek, A. Kay, S. M. Zakeeruddin and M. Grätzel, *Prog. Photovoltaics*, 2006, **14**, 589–601.
31 M. V. Khenkin, E. A. Katz, A. Abate, G. Bardizza, J. J. Berry, C. Brabec, F. Brunetti, V. Bulović, Q. Burlingame, A. Di Carlo, R. Cheacharoen, Y.-B. Cheng, A. Colsmann, S. Cros, K. Domanski, M. Dusza, C. J. Fell, S. R. Forrest, Y. Galagan, D. Di Girolamo, M. Grätzel, A. Hagfeldt, E. von Hauff, H. Hoppe, J. Kettle, H. Köbler, M. S. Leite, S. Liu, Y.-L. Loo, J. M. Luther, C. Q. Ma, M. Madsen, M. Manceau, M. Matheron, M. McGehee, R. Meitzner, M. K. Nazeeruddin, A. F. Nogueira, Ç. Odabaşı, A. Osherov, N.-G. Park, M. O. Reese, F. De Rossi, M. Saliba, U. S. Schubert, H. J. Snaith, S. D. Stranks, W. Tress, P. A. Troshin, V. Turkovic, S. Veenstra, I. Visoly-Fisher, A. Walsh, T. Watson, H. Xie, R. Yıldırım, S. M. Zakeeruddin, K. Zhu and M. Lira-Cantu, *Nat. Energy*, 2020, **5**, 35–49.
32 B. Ecker, H.-J. Egelhaaf, R. Steim, J. Parisi and E. von Hauf, *J. Phys. Chem. C*, 2012, **116**, 16333–16337.
33 R. García-Rodríguez, R. Jiang, E. J. Canto-Aguilar, G. Oskam and G. Boschloo, *Phys. Chem. Chem. Phys.*, 2017, **19**, 32132–32142.
34 I. Jerman, V. Jovanovski, A. Š. Vuk, S. B. Hočevar, M. Gaberščček, A. Jesih and B. Orel, *Electrochim. Acta*, 2008, **53**, 2281–2288.
35 G. N. R. Tripathi, R. H. Schuler and R. W. Fessenden, *Chem. Phys. Lett.*, 1985, **113**, 563–568.
36 K. R. Loos and A. C. Jones, *J. Phys. Chem.*, 1974, **78**, 2306–2307.
37 D. Tristant, P. Puech and I. C. Gerber, *Phys. Chem. Chem. Phys.*, 2015, **17**, 30045–30051.
38 M. A. Tadayyoni, P. Gao and M. J. Weaver, *J. Electroanal. Chem.*, 1986, **198**, 125–136.
39 S. Wang, Z. Huang, X. Wang, Y. Li, M. Günther, S. Valenzuela, P. Parikh, A. Cabreros, W. Xiong and Y. S. Meng, *J. Am. Chem. Soc.*, 2018, **140**, 16720–16730.
40 C. Law, S. C. Pathirana, X. Li, A. Y. Anderson, P. R. F. Barnes, A. Listorti, T. H. Ghaddar and B. C. O'Regan, *Adv. Mater.*, 2010, **22**, 4505–4509.
41 F. Bella, L. Porcarelli, D. Mantione, C. Gerbaldi, C. Barolo, M. Grätzel and D. Mecerreyes, *Chem. Sci.*, 2020, **11**, 1485–1493.
42 Y. Cao, Y. Saygili, A. Ummadisingu, J. Teuscher, J. Luo, N. Pellet, F. Giordano, S. M. Zakeeruddin, J.-E. Moser, M. Freitag, A. Hagfeldt and M. Grätzel, *Nat. Commun.*, 2017, **8**, 15390.
43 I. Mora-Seró, J. Bisquert, F. Fabregat-Santiago, G. Garcia-Belmonte, G. Zoppi, K. Durose, Y. Proskuryakov, I. Oja, A. Belaidi, T. Dittrich, R. Tena-Zaera, A. Katty, C. Lévy-Clément, V. Barrioz and S. J. C. Irvine, *Nano Lett.*, 2006, **6**, 640–650.